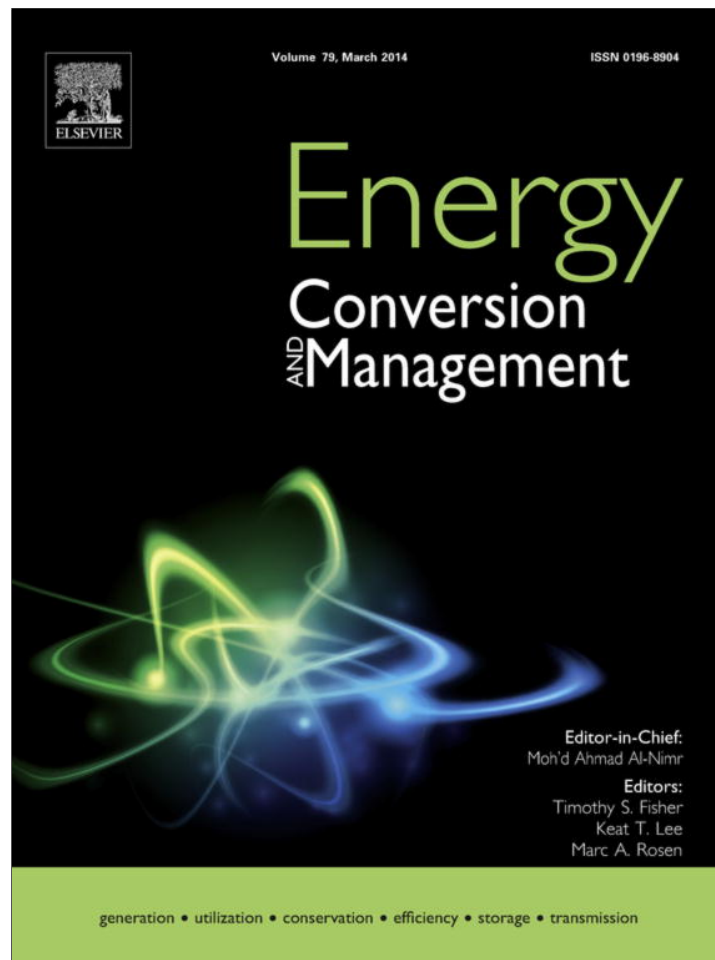


Provided for non-commercial research and education use.
Not for reproduction, distribution or commercial use.



This article appeared in a journal published by Elsevier. The attached copy is furnished to the author for internal non-commercial research and education use, including for instruction at the authors institution and sharing with colleagues.

Other uses, including reproduction and distribution, or selling or licensing copies, or posting to personal, institutional or third party websites are prohibited.

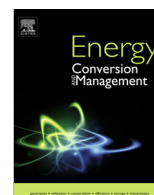
In most cases authors are permitted to post their version of the article (e.g. in Word or Tex form) to their personal website or institutional repository. Authors requiring further information regarding Elsevier's archiving and manuscript policies are encouraged to visit:

<http://www.elsevier.com/authorsrights>



Contents lists available at ScienceDirect

Energy Conversion and Management

journal homepage: www.elsevier.com/locate/enconman

The influence of gas radiation on the thermal behavior of a 2D axisymmetric turbulent non-premixed methane–air flame



Felipe Roman Centeno^a, Cristiano Vitorino da Silva^b, Francis H.R. França^{a,*}

^a Federal University of Rio Grande do Sul, Rua Sarmento Leite, no. 425, CEP 90050-170 Porto Alegre, RS, Brazil

^b Department of Engineering and Computer Sciences, Regional Integrated University of Alto Uruguai and Missions, URI, Sete de Setembro Avenue, no. 1621, CEP 99700-000 Erechim, RS, Brazil

ARTICLE INFO

Article history:

Received 6 October 2013

Accepted 17 December 2013

Available online 11 January 2014

Keywords:

Radiation heat transfer

WSGG model

Combustion

Turbulent non-premixed flames

Turbulence–radiation interactions

ABSTRACT

This paper presents a study of the effect of thermal radiation in the simulation of a turbulent, non-premixed methane–air flame. In such a problem, two aspects need to be considered for a precise evaluation of the thermal radiation: the turbulence–radiation interactions (TRI), and the local variation of the radiative properties of the participating species, which are treated here with the weighted-sum-of-gray-gases (WSGG) model based on newly obtained correlations from HITEMP2010 database. The chemical reactions rates were considered as the minimum values between the Arrhenius and Eddy Break-Up rates. A two-step global reaction mechanism was used, while the turbulence modeling was considered via standard $k-\epsilon$ model. The source terms of the energy equation consisted of the heat generated in the chemical reaction rates as well as in the radiation exchanges. The discrete ordinates method (DOM) was employed to solve the radiative transfer equation (RTE), including the TRI. Comparisons of simulations with/without radiation (which in turn was solved with/without TRI) demonstrated that the temperature, the radiative heat source, and the wall heat flux were importantly affected by thermal radiation, while the influence on species concentrations proved to be negligible. Inclusion of thermal radiation led to results that were closer to experimental data available in the literature for the same test case considered in this paper. Inclusion of TRI improved the agreement, although in a smaller degree. The main influence of TRI was mainly on global results, such as the peak temperature and the radiant fraction. The results show the importance of thermal radiation for an accurate prediction of the thermal behavior of a combustion chamber.

© 2013 Elsevier Ltd. All rights reserved.

1. Introduction

In non-premixed flames, the fuel and oxidant are initially separated, and the combustion is controlled by diffusion and turbulence. Combustion problems involve a number of coupled phenomena, such as fluid mechanics, heat transfer, and chemical kinetics of gaseous species and soot, in which thermal radiation can be the dominant heat transfer mode. Heat transfer directly affects the temperature field and, therefore, the chemical kinetics, which are strongly dependent on temperature. Therefore, an accurate description of radiative heat transfer is of great importance for simulations of combustion systems. On the other hand, modeling thermal radiation exchanges in combustion gases (such as water vapor and carbon dioxide) is a difficult task due to the highly complex dependence of the absorption coefficient with the wavenumber, which is typically characterized by hundreds of thousands or millions of spectral lines. Thus, the integration of the radiative

transfer equation (RTE) over the spectrum would be very expensive or even impossible without the use of spectral or global models. As a first simplification, the RTE is frequently solved with the gray gas (GG) model, where the dependence of the absorption coefficient over the wavenumber is simply neglected. In order to provide realistic results, more refined models are however needed. As one advance to the GG model, the weighted-sum-of-gray-gases (WSGG) [1] makes perhaps the best compromise between accuracy and computation demand, especially in global simulation of combustion processes in which the RTE is solved together with fluid flow, chemical kinetics and energy equation. In the WSGG model the entire spectrum is represented by a few bands having uniform absorption coefficients, each band corresponding to a gray gas. The weighting coefficients account for the contribution of each gray gas, and can be interpreted as the fractions of the blackbody energy in the spectrum region where the gray gases are located. In practice, those coefficients are obtained from fitting total emittances computed from experimental-gas-data, such as those presented in [2,3]. In a recent study, Demarco et al. [4] assessed several radiative models, such as the narrow band, wide band, GG and global models such as the WSGG and spectral-line-based WSGG (SLW).

* Corresponding author. Tel.: +55 51 3308 3360.

E-mail addresses: frcenteno@mecanica.ufrgs.br (F.R. Centeno), cristiano@uricer.edu.br (C.V. da Silva), frfranca@mecanica.ufrgs.br (F.H.R. França).

Nomenclature

$a_j(T)$	emission weighted factor (WSGG)	S^ϕ	source term for ϕ
c	each reaction mechanism	T'	temperature fluctuation
C_{TRI}	constant of the TRI model	T'^2	temperature variance
C_T	constant of the TRI model	$T_{ref,\alpha}$	reference temperature of α
$C_{1,\epsilon}, C_{2,\epsilon}$	constants of the turbulence model	T_w	wall temperature
C_μ	constant of the turbulence model	x	species molar fraction
f_{rad}	radiant fraction		
h_α^0	formation enthalpy of species α	Greek symbols	
$I_b(I_{b\eta})$	black body (spectral) intensity	α	each chemical species
I	radiation intensity fluctuation	ϵ	dissipation rate of k
j	each gray gas of the WSGG model	ϕ	generic variable
k	turbulent kinetic energy	Γ_ϕ	diffusive coefficient for ϕ
κ_j	absorption coefficient for the j th gray gas for WSGG model	κ'_ϕ	absorption coefficient fluctuation
N_G	number of gray gases (WSGG)	μ_t	turbulent viscosity
p^*	modified pressure	μ, ζ, ξ	discrete ordinates method directions
Pr_t, Sc_t	turbulent Prandtl and Schmidt numbers	η	wavenumber
\bar{q}_r	radiative heat flux	$\sigma_k, \sigma_\epsilon$	Prandtl numbers for k and ϵ
R_α	volumetric rate of formation or consumption of α		
S_{rad}	radiative heat source		

According to the authors, the WSGG is very efficient from a computational point of view, and can yield accurate predictions, although significant discrepancies can appear in high soot loadings. Simplified radiative property models, such as the WSGG or GG models, are often used in computational fluid dynamics (CFD) to simulate combustion problems. The main reason is that implementing more sophisticated models may become excessively time consuming when fluid flow/combustion/radiative heat transfer are coupled. Examples of works applying those models can be found in Watanabe et al. [5], where it was presented a numerical simulation of turbulent spray combustion to predict the combustion behavior in a jet burner taking into account thermal radiation by means of the WSGG model; in Bidi et al. [6], where the RTE was solved using the WSGG model to compute non-gray radiation in combustion gases in a cylindrical chamber; in Bazdidi-Tehrani and Zeinivand [7], who investigated a two-phase reactive flow corresponding to a diesel oil–air flame to predict the turbulent flow behavior and the temperature distribution; and the investigation on the effect of turbulence and radiation models on combustion characteristics in propane–hydrogen diffusion flames reported in Yilmaz et al. [8]. Crnomarkovic et al. [9] compared the numerical results obtained when the GG and the WSGG models were applied to model the radiative properties of the gas phase inside a lignite fired furnace. In Yadav et al. [10] the combustion processes of turbulent non-premixed pilot stabilized flames were studied including radiative heat transfer by means of the WSGG model. In Silva et al. [11], the authors applied the GG model to study the combustion of coal in a commercial thermal power plant to simulate the operational conditions and identify the factors of inefficiency.

Several researchers have studied new WSGG correlations for application in combustion systems. Taking into account that a limitation of the WSGG is that its correlations coefficients are established for particular ratio of partial pressures for CO_2 and H_2O mixtures, Krishnamoorthy [12] obtained new WSGG parameters computed from total emissivity correlations encompassing the range of the $\text{H}_2\text{O}/\text{CO}_2$ ratios encountered within Sandia Flame D. Predictions from the new model compared favorably against the SLW model and existing benchmarks. With the same motivation, Johansson et al. [13] modified the WSGG to account for various ratios of H_2O and CO_2 concentrations, covering from oxyfuel combustion of coal, with dry or wet flue gas recycling, as well as

combustion of natural gas. The modified WSGG model significantly improved the estimation of the radiative source term compared to gray models, while the accuracy of wall fluxes was similar to gray models or better.

One important advance in the modeling of radiation in participating gas was the establishment in the past century of high-resolution spectral database that provide spectroscopic parameters to generate the transition lines, such as HITRAN, built at a reference temperature of 296 K for atmospheric applications, and HITEMP, which was established for high temperature applications. Recently, HITEMP 2010 [14] was released as a major improvement of previous versions, expanding the number of transition lines for H_2O and CO_2 , and also allowing for application in temperatures up to 4000 K. In recent works, Kangwanpongpan et al. [15] considered the determination and evaluation of new correlations for the WSGG model, fitted from emittance charts calculated from the up-to-date HITEMP 2010 database, to predict the radiative transfer in gases under oxyfuel conditions, while Dorigon et al. [16] generated correlations for typical products of the combustion of methane and fuel oil.

Another aspect to be considered in turbulent combustion simulations is the so-called turbulence–radiation interactions (TRI). Turbulence and radiation are physical phenomena of high complexity even when analyzed independently. In turbulent flow, it is not possible to deal with these phenomena in an independent way, but in a coupled form. In turbulent reactive flows, temperature and species concentration fields can undergo high levels of fluctuations, leading to variations on the radiative field, which in turn affects the temperature field and, consequently, the scalar fluctuations. Therefore, turbulence influences radiation, and vice-versa, but the influence of radiation on turbulence is relatively less important [17].

The first theoretical investigation on TRI [18] showed that radiative properties of a turbulent flame would be incorrectly predicted if turbulent fluctuations were neglected from calculations, especially for high optical thickness mediums. Those results were experimentally confirmed later in [19,20].

Numerical simulations of TRI can be decoupled or coupled. Decoupled calculations consider temperature and species concentrations distributions as inputs, i.e., they are taken from previous CFD solutions or from experimental data. Coupled calculations

consider simultaneously all flow mechanisms, such as turbulence, heat transfer and combustion, so they are considerably more complex than the former. Decoupled calculations were presented in Hall and Vranos [21], where results obtained from time-averaged RTE solution were compared to those obtained from a stochastic method for an one-dimensional problem; Krebs et al. [22] studied TRI effect on radiation intensity from CO₂; in a following work, Krebs et al. [23] focused on propane–air flames with the objective of analyzing the influence of temperature and species concentration fluctuations; Coelho [24,25] evaluated the accuracy of the *optically thin fluctuation approximation* (OTFA) [26] by comparing results obtained with this approximation and results from exact solutions of RTE. The first coupled calculation of radiative transfer in reactive flow to investigate TRI was reported in Song and Viskanta [27], in which property functions were prescribed for the combustion gases. The most recent literature has been focused on analyzing the most important TRI correlations (temperature self-correlation, absorption coefficient–temperature correlation, absorption coefficient self-correlation, and absorption coefficient–radiation intensity correlation). Some examples of coupled investigations were reported in Li and Modest [28], Habibi et al. [29], Poitou et al. [30] and Gupta et al. [31]. Results pointed that the absorption coefficient–temperature correlation and the temperature self-correlation are the most important TRI terms in reactive flows [28,31–33]. Furthermore, it was found in Gupta et al. [31] and in Modest and Mehta [34] that the absorption TRI term (correlation between absorption coefficient and radiation intensity fluctuations, which is neglected in OTFA) is important only for optically thick medium.

This study presents a numerical RANS (Reynolds Average Navier–Stokes) simulation of turbulent non-premixed methane–air flame in a cylindrical combustion chamber taking into account radiation effect of non-gray gases by means WSGG correlations [16] generated from HITEMP 2010 database [14] and including TRI [35], with the objective of evaluating the influence of radiation on the overall thermal behavior. For evaluation of the proposed solution, the case described in [36] was studied, since detailed spatial distributions measurements are available for the main gas species concentrations and for the temperature field.

2. Problem statement

The physical system consists of the natural gas combustion chamber described in [36], which presents several challenges for radiation modeling in the sense that the flame is turbulent, and with highly non-isothermal, non-homogeneous medium. Several experimental data for temperature and species concentrations profiles along axial and radial coordinates were presented in [36], in addition to the results provided in the investigations of [37–39], making it a good test case for the methodology that is presented in the current study.

Keeping the same conditions as described in [36], the cylindrical chamber has length and diameter of 1.70 m and 0.5 m, respectively, as shown in Fig. 1. Natural gas is injected into the chamber by a duct aligned with the chamber centerline, leading

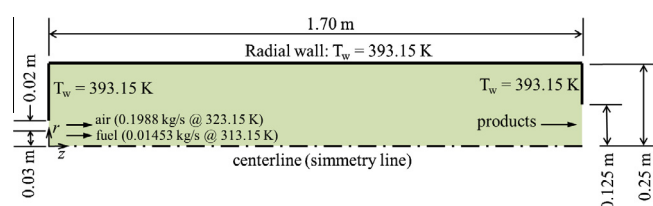


Fig. 1. Combustion chamber geometry.

to a non-swirling flame. The burner provides the necessary amount of air and natural gas as required by the process. In all cases a fuel excess of 5% (equivalence ratio of 1.05) was prescribed. For a fuel mass flow rate of 0.01453 kg/s at a temperature of 313.15 K, this requires an air mass flow rate of 0.1988 kg/s, at a temperature of 323.15 K. The fuel enters the chamber through a cylindrical duct having 0.06 m diameter, while air enters the chamber through a centered annular duct having a spacing of 0.02 m. For such mass flow rates, the fuel and air velocities are 7.23 and 36.29 m/s, respectively. The Reynolds number at the entrance, approximately 1.8×10^4 , points that the flow is turbulent. The inlet air is composed of oxygen (23% in mass fraction), nitrogen (76%) and water vapor (1%), while the fuel is composed of 90% of methane and 10% of nitrogen. The burner power is about 600 kW. The fan and the other external components are not included in the computational domain, although their effects are taken into account through the inlet flow conditions. Buoyancy effects are neglected due to the high velocities that are provided by the burner. Fig. 1 also depicts the thermal boundary conditions of the cylindrical chamber: symmetry in the centerline, and prescribed temperature on the walls, equal to 393.15 K. In addition, impermeability and no-slip conditions were assumed on the walls. In the symmetry line, it was assumed that both the radial velocity and the velocity gradient were null. The same null gradient in the symmetry line was adopted for the turbulent kinetic energy and its dissipation rate, enthalpy, and species concentrations. In the outlet, null diffusive fluxes were assumed for all variables, the axial velocity component was corrected by a factor to satisfy mass conservation, and the radial velocity was imposed to be null. The chamber walls, the inlet and the outlet were modeled as black surfaces. The temperature at the inlet duct was specified to be at the fuel and oxidant temperatures, while the temperature of the chamber outlet was set equal to the outlet flow bulk temperature, T_{bulk} , as given by:

$$T_{\text{bulk}} = \frac{\int_A \rho u c_p T dA}{\int_A \rho u c_p dA} \quad (1)$$

In the inlet, the velocity and concentration profiles were assumed uniform in the axial direction, while the turbulent kinetic energy was computed as $k = 3/2(u_{\text{in}} i)^2$, where i is the turbulence intensity (prescribed as 6% and 10% for the air and for the fuel streams, respectively) and u_{in} is the inlet axial mean velocity. For the turbulent kinetic energy dissipation rate, the relation $\varepsilon = (C_{\mu}^{3/4} k^{3/2})/l$ was employed, where l is the turbulence characteristic length scale (taken as 0.04 m and 0.03 m for the air and the fuel streams, respectively). For both energy and momentum conservation equations, standard wall functions were applied at wall, taking into account the viscous layer dominated by molecular diffusion close to the walls [40].

3. Mathematical formulation

The proposed work is stated as: considering a steady turbulent non-premixed methane–air flame in a cylindrical chamber, compute the temperature, species concentrations and velocity fields, and verify the influence of radiation on the process, taking into account the WSGG model based on HITEMP 2010 data [16] and TRI effects [35].

3.1. Governing equations

Considering the conservation equation for steady incompressible flow in 2D axisymmetric coordinates for the generic variable ϕ , Eq. (2), the mass, momentum in the axial and radial directions, k – ε turbulence model, energy, and chemical species conservation

Table 1
Generic variable, diffusive coefficient, source terms for the conservation equations.

Equation	ϕ	Γ_ϕ	S^ϕ
Continuity	1	0	0
Axial momentum	u	$(\mu + \mu_t)$	$-\frac{\partial p}{\partial z} + \frac{\partial}{\partial z}(\mu_t \frac{\partial u}{\partial z}) + \frac{1}{r} \frac{\partial}{\partial r}(r \mu_t \frac{\partial v}{\partial z})$
Radial momentum	v	$(\mu + \mu_t)$	$-\frac{\partial p}{\partial r} + \frac{\partial}{\partial z}(\mu_t \frac{\partial v}{\partial r}) + \frac{1}{r} \frac{\partial}{\partial r}(r \mu_t \frac{\partial v}{\partial r}) - \frac{(\mu + \mu_t)v}{r^2} + \frac{\rho w^2}{r^2}$
Turbulent kinetic energy	k	$(\mu + \frac{\mu_t}{\sigma_k})$	$[\mu_t (2(\frac{\partial u}{\partial z})^2 + (\frac{\partial u}{\partial r} + \frac{\partial v}{\partial z})^2 + 2(\frac{\partial v}{\partial r})^2 + 2(\frac{v}{r})^2)] - \rho \epsilon$
Turbulent kinetic energy dissipation	ϵ	$(\mu + \frac{\mu_t}{\sigma_\epsilon})$	$C_{1,\epsilon} [\mu_t (2(\frac{\partial u}{\partial z})^2 + (\frac{\partial u}{\partial r} + \frac{\partial v}{\partial z})^2 + 2(\frac{\partial v}{\partial r})^2 + 2(\frac{v}{r})^2)] \frac{\epsilon}{k} - C_{2,\epsilon} \frac{\epsilon^2}{k}$
Energy	h	$(\frac{\mu}{Pr} + \frac{\mu_t}{Pr_t})$	$S_{rad} + \sum_\alpha [h_\alpha^0 + \int_{T_{ref,\alpha}}^T c_{p,\alpha} dT] R_\alpha$
CH ₄ , O ₂ , CO ₂ , CO and H ₂ O mass fraction	y_α	$(\frac{\mu}{Sc} + \frac{\mu_t}{Sc_t})$	R_α

equations can be determined by choosing ϕ , Γ_ϕ , and source term S^ϕ from Table 1.

$$\frac{\partial}{\partial z}(\rho u \phi - \Gamma_\phi \frac{\partial \phi}{\partial z}) + \frac{1}{r} \frac{\partial}{\partial r}(r \rho v \phi - r \Gamma_\phi \frac{\partial \phi}{\partial r}) = S^\phi \quad (2)$$

The following variables are used in Table 1: z and r are the axial and radial coordinates [m], u and v are the velocities in these respective directions [m/s], w is the angular velocity [m/s], ρ is the density of the gaseous mixture [kg/m³], μ is the gaseous mixture dynamic viscosity, and μ_t is the turbulent viscosity [Ns/m²], defined as $\mu_t = C_\mu \rho k^2 / \epsilon$. The term $p^* = p - (2/3)k$ is the modified pressure [Pa], C_μ is an empirical constant of the turbulence model ($C_\mu = 0.09$), p is the combustion chamber operational pressure ($p = 101325$ Pa [41]), and k [m²/s²] and ϵ [m²/s³] are the turbulent kinetic energy and its dissipation. Also, $C_{1,\epsilon}$ and $C_{2,\epsilon}$ are empirical constants of the turbulence model ($C_{1,\epsilon} = 1.44$ and $C_{2,\epsilon} = 1.92$), σ_k and σ_ϵ are the Prandtl numbers of the kinetic energy and dissipation, respectively ($\sigma_k = 1.0$ and $\sigma_\epsilon = 1.3$). Pr_t and Sc_t are the turbulent Prandtl and Schmidt numbers, R_α [kg/(m³ s)] is the volumetric rate of formation or consumption of the α th chemical species (CH₄, O₂, CO₂, CO, H₂O) (this term is briefly discussed in Section 3.2). T is the temperature of the gaseous mixture [K]. \bar{M}_α [kg/kmol], $c_{p,\alpha}$ [kJ/(kg K)], h_α^0 [J/kg] and $T_{ref,\alpha}$ [K] are the molecular mass, the specific heat, the formation enthalpy and the reference temperature of each α th chemical species. S_{rad} [W/m³] is the radiative heat source term, computed as the negative divergence of the radiative heat flux (discussed in Section 3.3).

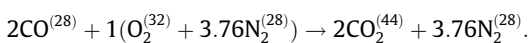
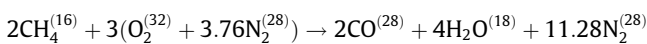
In addition to the conservation laws presented in Table 1, an equation of state is required to calculate the mixture density. Considering the mixture of fuel, oxidant and products as an ideal gas, the equation of state can be written as,

$$\rho = \frac{p}{RT} \sum_\alpha \frac{y_\alpha}{\bar{M}_\alpha} \quad (3)$$

where \bar{R} is the universal gas constant ($\bar{R} = 8.314$ kJ/(kmol · k)), y_α [kg _{α} /kg_{tot}] is the mean mass fraction of each α th chemical species. Also, it is important to note that in the present work all quantities (as u , v , h , T , c_p , y_α , ρ , R_α , S_{rad} , etc.) are time-averaged (mean), but they are not written with an overbar (usual in RANS simulations) in order to not confuse with molar quantities.

3.2. Combustion kinetics

As a basic assumption, it is considered that the combustion process occurs at finite rates with methane oxidation taking two global steps:



The rate of formation or consumption, $R_{\alpha,c}$, of each α th species in each c th reaction (there are two reactions in the present study, so $c = 2$) is obtained by the Arrhenius–Magnussen’s model [42–44],

in which the rate of formation or consumption of the chemical species are taken as the smallest one between the values obtained from Arrhenius kinetics or from Magnussen’s equations (Eddy Break-Up) [45]. In Magnussen’s model, the chemical reaction rate is governed by the large-eddy mixing time scale, k/ϵ , while combustion proceeds whenever turbulence is present ($k/\epsilon > 0$). In the model, the Arrhenius rate act as a kinetic “switch”; once the flame is ignited, the Magnussen’s rate is generally smaller than the Arrhenius rate, so reactions are mixing-limited [44]. The investigation in Silva et al. [37], which considered the same combustion chamber, provided the relative importance of the combustion kinetics by computing the Damköhler number, and found that the combustion process is governed by Arrhenius rates in the flame core and by Magnussen’s rates in all the other regions. This formulation was also successfully employed in [37,39].

While the two-equation chemistry assumption has been used with great success in combustion modeling, it should be recognized that detailed reaction mechanisms effects may be very important in several practical applications, especially those involving flame ignition and extinction, or those involving predictions of minor species such as soot, NO and other radicals, which are not the aim of the present work. Also, the chemistry presented above does not involve soot formation/oxidation, considering that the methane flame is expected to produce low quantities of soot. In a simulation of a turbulent, non-premixed methane–air flame conducted in Woolley and Yunardi [46], it was found a maximum soot volume fraction of 0.15 ppm. However, it should be recognized that even small quantities of soot can affect the radiation heat transfer, so the inclusion of soot into the analysis would be one possible future advance in the research. In an investigation of several turbulent reactive flows [47] it was found that the contributions of gases and soot to radiative heat transfer corresponded to approximately 90% and 10%, respectively, for a flame similar to the one studied here. As for the present study, considering only gas radiation permits assessing the effect of the gas radiation in a turbulent methane flame. The proper understanding of the gas radiation is an important step prior to investigations including both gaseous species and soot.

The average volumetric rates of formation or consumption of the α th chemical species, R_α , which appears in both the energy and species mass fraction equations, are then computed from the summation of the volumetric rates of formation or consumption in all the c th reactions where the α th species is present, i.e., $R_\alpha = \sum c R_{\alpha,c}$.

3.3. Radiation modeling

The radiative transfer equation (RTE) for non-scattering media, in cylindrical coordinates, with the discrete ordinates method (DOM), is given by:

$$\frac{\partial I_\eta}{\partial s} = \mu \frac{\partial I_\eta}{\partial r} + \zeta \frac{\partial I_\eta}{\partial z} - \frac{\zeta}{r} \frac{\partial I_\eta}{\partial \varphi} = -\kappa_\eta I_\eta + \kappa_\eta I_{\eta b} \quad (4)$$

subjected to boundary conditions for diffusively emitting and reflecting opaque surface:

$$I_{\eta w} = \varepsilon_{\eta w} I_{\eta b}(T_w) + \frac{(1 - \varepsilon_{\eta w})}{\pi} \int_{\hat{n} \cdot \hat{s}} I_{\eta} |\hat{n} \cdot \hat{s}| d\Omega \quad (5)$$

where μ , ζ , and ξ are the directions, η is the wavenumber, $I_{\eta b}$ is the blackbody spectral intensity, I_{η} is the intensity, $\varepsilon_{\eta w}$ is the wall emissivity, \hat{n} and \hat{s} are the vector normal to the surface element and the vector in the direction of the radiation intensity, respectively, Ω is the solid angle, T_w is the wall temperature, and κ_{η} is the spectral absorption coefficient. In the right side of Eq. (4), the first and the second terms represent, respectively, attenuation due to absorption and augmentation due to emission. Once the RTE is solved, the radiative heat source, presented in the energy equation as S_{rad} , is calculated as:

$$S_{rad} = -\nabla \cdot \bar{q}_r = \int_{\Omega} \int_{\eta} (\kappa_{\eta} I_{\eta} - \kappa_{\eta} I_{b\eta}) d\eta d\Omega \quad (6)$$

where \bar{q}_r is the radiative heat flux.

The spectral absorption coefficient (κ_{η}) is strongly dependent on the wavenumber, which for participating gases can involve several thousands or millions of spectral lines. Therefore, solving Eq. (4) for all spectral lines is in general excessively time-consuming for coupled solutions of the conservation equations. As such, gas models have been developed to solve the RTE quickly. A brief description of the gas model selected for the present analysis, the WSGG model, is presented in Section 3.4.

3.4. The weighted-sum-of-gray-gases (WSGG) model

The original formulation of the WSGG model [1] consists of expressing the total gas emittance by weighted-sum-of-gray-gas emittances. The emission weighted factors, $a_j(T)$, and the absorption coefficients, κ_j , for the j th gray gas are in general determined from the best fit of the total emittance with the constraint that the a_j must sum to 1. From a more general point of view, the WSGG model can be applied as a non-gray gas model [48], solving the RTE for the N_G (number of gray gases) plus one ($j = 0$, representing spectral windows where H_2O and CO_2 are transparent to radiation) for a clear gas:

$$\frac{dI_j}{ds} = -\kappa_j I_j + \kappa_j a_j(T) I_{b_j}(T) \quad (7)$$

in which the emission weighted factor $a_j(T)$ is given by,

$$a_j(T) = \sum_{i=1}^5 b_{j,i} T^{i-1} \quad (8)$$

with j varying from 0 to N_G , and $I = \sum_{j=0}^{N_G} I_j$. The functional dependence of the weighted factors with temperature is generally fitted by polynomials, Eq. (8), where the polynomial coefficients ($b_{j,i}$) as well as the absorption coefficients for each gray gas can be tabulated. For H_2O/CO_2 mixtures, these coefficients are generally established for particular ratios of the partial pressure, p_{H_2O}/p_{CO_2} , which could limit the application of the method. In the present study the weighted factors polynomial coefficients and absorption coefficients were taken from Dorigon et al. [16] for $p_{H_2O}/p_{CO_2} = 2$. Such

WSGG correlations were fitted from HITEMP 2010 [14], which is the most recent molecular spectroscopic database for high temperatures. In the same study, Dorigon et al. [16], compared results obtained with the new coefficients against line-by-line (LBL) benchmark calculations for one-dimensional non-isothermal and non-homogeneous problems, finding consistently satisfactory agreement between the LBL and WSGG solutions, with maximum and average errors of about 5% and 2% for different test cases. For convenience, Table 2 shows the pressure absorption coefficient $\kappa_{p,j}$ and coefficients $b_{j,i}$ obtained in [16]. The absorption coefficient of each gray gas in Eq. (7) can be computed from the pressure absorption coefficient by the following relation:

$$\kappa_j = p_{CO_2+H_2O} \times \kappa_{p,j} \quad (9)$$

where $p_{CO_2+H_2O}$ is the local partial pressure of CO_2 and H_2O . This is one important aspect of the WSGG model, for it allows its ready application to non-homogeneous problems, in which the local partial pressure of the participating species varies from point to point in the computation domain. Centeno et al. [49] tested the coefficients presented in Table 2 against old ones presented in [2] for an axisymmetric cylindrical combustion chamber, and found the new coefficients to make better agreement with experimental data. It is assumed here that the contribution from other radiating species, such as CO and CH_4 , is negligible. The contribution from CO in the combustion gases is negligible, since its molar concentration is not expected to exceed 0.1%, while the contribution from CH_4 is even lower [50].

3.5. Turbulence–radiation interactions

The radiative transfer equation (RTE), Eq. (4), is applicable to instant quantities that fluctuate in a turbulent flow, while the RANS turbulence model can only provide time-averaged (mean) quantities and, possibly, their mean square fluctuations. Considering the spectrally integrated form of the RTE, and time averaging it, results in:

$$\frac{d\bar{I}}{ds} = -\bar{\kappa}\bar{I} + \bar{\kappa}\bar{I}_b \quad (10)$$

Decomposition of variables (temperature and species concentrations) into mean and fluctuating components followed by time-averaging reveals several terms which require modeling [51]:

- temperature self-correlation, $\overline{T^4}$, or related mean values that depend only on the temperature, such as \bar{I}_b and $\bar{I}_{b\eta}$;
- absorption coefficient self-correlation, $\bar{\kappa}$, or similar correlations that depend only on the radiative properties of the medium;
- absorption coefficient-temperature correlation, $\overline{\kappa T^4}$, or analogous ones, such as $\overline{\kappa_j a_j \bar{I}_b}$;
- absorption coefficient-radiation intensity correlation, $\overline{\kappa I}$, or analogous ones, such as $\overline{\kappa_j \bar{I}_j}$.

The absorption coefficient-radiation intensity correlation, i.e., the first term in the right hand of Eq. (10), is expressed as $\overline{\kappa I} = \bar{\kappa}\bar{I} + \overline{\kappa' I'}$. Several studies have neglected the second term on

Table 2
WSGG model coefficients [16], $p_{H_2O}/p_{CO_2} = 2$.

j	$\kappa_{p,j} \text{ (m}^{-1} \text{ atm}^{-1}\text{)}$	$b_{j1} \times 10^1$	$b_{j2} \times 10^4 \text{ (K}^{-1}\text{)}$	$b_{j3} \times 10^7 \text{ (K}^{-2}\text{)}$	$b_{j4} \times 10^{10} \text{ (K}^{-3}\text{)}$	$b_{j5} \times 10^{14} \text{ (K}^{-4}\text{)}$
1	0.192	0.5617	7.8440	−8.5630	4.2460	−7.4400
2	1.719	1.4260	1.7950	−0.1077	−0.6972	1.7740
3	11.370	1.3620	2.5740	−3.7110	1.5750	−2.2670
4	111.016	1.2220	−0.2327	−0.7492	0.4275	−0.6608

the right hand side of this expression ($\overline{\kappa'T}$) based on arguments of Kabashnikov and Kmit [26], known as the OTFA, and relies on the assumption that the absorption coefficient fluctuations are weakly correlated with the radiation intensity fluctuations, i.e., $\overline{\kappa'T} \approx 0$, if the mean free path for radiation is much larger than turbulence integral length scale. According to the literature [51], the OTFA is not generally valid over the entire spectrum, particularly at the center of strong spectral lines of absorbing gases. However, it is believed that the spectral regions where this approximation does not hold plays minor influence on the total radiation intensity, in this manner it is justifiable for the vast majority of engineering applications, with the possible exception of strongly sooty flames. Thus, the OTFA has been employed in most studies dealing with TRI based on time-averaged form of the RTE [21,25,28,30,32,35]. Introducing this approximation into Eq. (10) results in

$$\frac{d\bar{I}}{ds} = -\bar{\kappa}\bar{I} + \overline{\kappa'I_b} \quad (11)$$

As for the second term in the right hand of Eq. (11), which is proportional to $\overline{\kappa'T^4}$, the instant values of κ and T correlate in a turbulent flow. In the present study, it is applied the approximation proposed in Snegirev [35], in which both the absorption coefficient-temperature correlation and the temperature self-correlation are considered. These two TRI correlations were found to be the most important in reactive flows [28,31–33]. Decomposition of temperature and absorption coefficient into average and fluctuating components, $T = \bar{T} + T'$ and $\kappa = \bar{\kappa} + \kappa'$, followed by time averaging, yields [35]:

$$\begin{aligned} \overline{\kappa'T^4} &= \overline{(\bar{\kappa} + \kappa')(\bar{T} + T')^4} \\ &= \bar{\kappa} \cdot \bar{T}^4 \left(1 + \underbrace{6 \frac{\overline{T'^2}}{\bar{T}^2} + 4 \frac{\overline{T'^3}}{\bar{T}^3} + \frac{\overline{T'^4}}{\bar{T}^4}}_{\text{temperature self-correlation}} + 4 \frac{\overline{\kappa'T'}}{\bar{\kappa} \cdot \bar{T}} + \underbrace{6 \frac{\overline{\kappa'T'^2}}{\bar{\kappa} \cdot \bar{T}^2} + 4 \frac{\overline{\kappa'T'^3}}{\bar{\kappa} \cdot \bar{T}^3} + \frac{\overline{\kappa'T'^4}}{\bar{\kappa} \cdot \bar{T}^4}}_{\text{absorption coefficient-temperature correlation}} \right) \end{aligned} \quad (12)$$

where the expression in brackets on the right allows for turbulent fluctuations. Only the correlations of the lowest order, $\overline{T'^2}$ and $\overline{\kappa'T'}$, are taken into account. The terms $\overline{T'^2}$ and $\overline{\kappa'T'}$ must be modeled by expressing them as functions of the averaged parameters of the flow. Species concentrations fluctuations play a minor role on TRI [33,50], although investigations have shown that their effects are not negligible, particularly when advanced spectral methods are applied for determination of radiative heat fluxes [25]. Therefore, neglecting species concentrations fluctuations to compute $\overline{\kappa'T'}$ in Eq. (12), Snegirev [35] replaced the dependence $\kappa(T) = \kappa(\bar{T} + T')$ by the Taylor series $\kappa \approx \kappa(\bar{T}) + T' \frac{\partial \kappa}{\partial T} \Big|_{\bar{T}} + \frac{T'^2}{2} \frac{\partial^2 \kappa}{\partial T^2} \Big|_{\bar{T}} + \dots$. Using the preceding Taylor series, the mean value, $\bar{\kappa}$, and the fluctuating component $\kappa' = \kappa - \bar{\kappa}$, the average of the product, $\overline{\kappa'T'}$, becomes $\overline{\kappa'T'} \approx \bar{T}^2 \frac{\partial \kappa}{\partial T} \Big|_{\bar{T}} + \frac{\overline{T'^3}}{2} \frac{\partial^2 \kappa}{\partial T^2} \Big|_{\bar{T}} + \dots \approx \bar{T}^2 \frac{\partial \kappa}{\partial T} \Big|_{\bar{T}}$. Neglecting higher order terms, Eq. (12) can be written as [35]:

$$\overline{\kappa'T^4} = \bar{\kappa} \cdot \bar{T}^4 \left(1 + C_{TRI} 6 \frac{\overline{T'^2}}{\bar{T}^2} + 4 \frac{\overline{T'^2}}{\bar{\kappa} \cdot \bar{T}} \frac{\partial \kappa}{\partial T} \Big|_{\bar{T}} \right) \quad (13)$$

Eq. (13) is used in this work as an approximate estimate for $\overline{\kappa'T^4}$ allowing for turbulent temperature fluctuations. The value for C_{TRI} was initially suggested by [35] from data fitting for T^4/\bar{T}^4 and $\overline{T'^2}/\bar{T}^2$ as presented in Burns [52], allowing the consideration of the temperature self-correlation into the current formulation, followed by an adjustment leading to a value of 2.5 for C_{TRI} .

To evaluate $\overline{T'^2}$, required for Eq. (13), the transport equation for temperature variance needs to be solved:

$$\begin{aligned} \frac{\partial}{\partial x} (\rho \bar{u} \overline{T'^2}) + \frac{1}{r} \frac{\partial}{\partial r} (r \rho \bar{v} \overline{T'^2}) &= \frac{\partial}{\partial x} \left(\left(\mu + \frac{\mu_t}{Pr_t} \right) \frac{\partial \overline{T'^2}}{\partial x} \right) \\ &+ \frac{1}{r} \frac{\partial}{\partial r} \left(r \left(\mu + \frac{\mu_t}{Pr_t} \right) \frac{\partial \overline{T'^2}}{\partial r} \right) \\ &+ 2 \frac{\mu_t}{\sigma_t} \left(\frac{\partial \bar{T}}{\partial z} + \frac{\partial \bar{T}}{\partial r} \right)^2 - C_T \rho \overline{T'^2} \frac{\varepsilon}{k} \end{aligned} \quad (14)$$

where $C_T = 2.0$ is the model constant. Eq. (14) must be solved together with the set of equations presented in Table 1, considering $\phi = \overline{T'^2}$, $\Gamma_\phi = \mu + \mu_t/Pr_t$ and S^ϕ equal to the two last terms in the right hand of Eq. (14). Also, in solving Eq. (14), $\overline{T'^2}$ was set as zero in the boundaries [35].

4. Results and discussions

The set of equations were solved using the finite volume method [40] by means of a Fortran code. The power-law was applied as the diffusive-advective interpolation function on the faces of the control volumes. The pressure-velocity coupling was made by the SIMPLE method. The resulting system of algebraic equations was solved by the TDMA algorithm, with block correction in all equations except the equations for k and ε . A grid with 90 volumes in the axial direction and 50 volumes in the radial direction was used. The numerical accuracy was checked comparing predicted results calculated using this grid with results obtained using coarser and thinner grids. As found, the 90×50 grid provided grid independent results, and required reasonable computational effort. The grid is non-uniformly spaced in the radial direction, and uniformly spaced in the axial direction. The radiative transfer calculations were performed using the same spatial grid, and S_6 quadrature. Convergence criteria were based on the imposition that the normalized residual mass in the SIMPLE method was 10^{-8} . For the other equations the maximum relative variation between iterations was 10^{-6} . The radiative transfer in molecular gases depends on the number of radiative participant molecules per unit of volume. According to Eq. (9), the pressure absorption coefficient for the j th gray gas for the WSGG model, $\kappa_{p,j}$ (in $\text{m}^{-1} \text{atm}^{-1}$), present in Table 2, was multiplied by the summation of the partial pressures of H_2O and of CO_2 for each computational volume cell, obtaining the absorption coefficient for the j th gray gas, κ_j (in m^{-1}), necessary to compute Eq. (7). In this manner, inhomogeneity of H_2O and CO_2 concentrations inside the combustion chamber was taken into account to compute the radiative transfer.

In order to study the effect of the gas radiation heat transfer inside the combustion chamber, three different scenarios were considered. In the first scenario, radiation was completely ignored in order to analyze the importance of radiation in this particular flame simulation. In the second and third scenarios, radiation was considered but with TRI computed solely for the third scenario, allowing an evaluation of TRI effects on the flame. Comparisons were made to verify how the different radiative scenarios affect the temperature, H_2O and CO_2 molar fractions, and radiative heat source fields, as well as some of the thermal quantities, such as the radiant fraction and heat fluxes through chamber walls.

Fig. 2 shows the results for temperature as well as for H_2O and CO_2 molar fraction distributions. On the left, Fig. 2(a–c) depict the temperature plots obtained for the three scenarios that were described above as well as the rms (root mean square) temperature

fluctuation values, computed as $\sqrt{\overline{T'^2}}$, Fig. 2(d). As seen, the rms temperature fluctuation reaches a local maximum of about 50% of the mean temperature. In the right, Fig. 2(e) and (f) shows the molar fraction distribution for the most important radiative chemical species, H_2O and CO_2 , while the ratio between these two quantities is shown in Fig. 2(g).

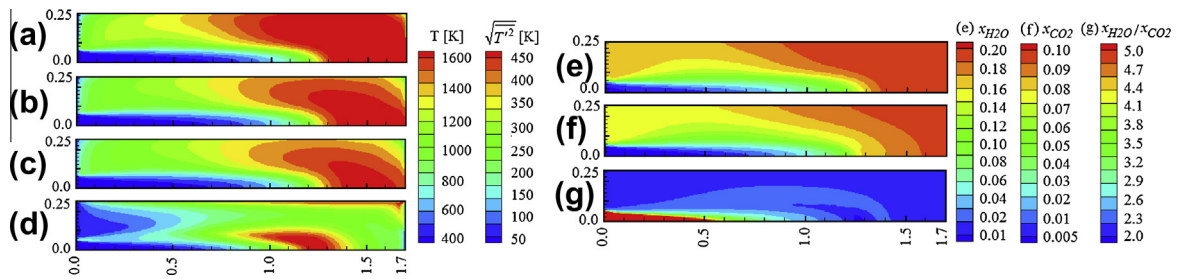


Fig. 2. Temperature fields: (a) radiation neglected; (b) radiation computed without TRI; (c) radiation with TRI; (d) temperature fluctuations, $\sqrt{T^2}$. Chemical species molar fraction fields: (e) H_2O ; (f) CO_2 ; and (g) ratio between molar fractions of H_2O and CO_2 .

As can be seen in Fig. 2(a–c), consideration of the radiative transfer and TRI played an important role in the temperature field. Computed flame peak temperatures were 1851 K, 1714 K and 1663 K for cases without radiation, and with radiation neglecting and considering TRI, respectively. While these peaks were local, they can be taken as a measure to characterize the entire temperature field. The decrease in the peak temperature as a result of neglecting or considering radiative transfer (ΔT_{RAD}), and of neglecting or considering TRI (ΔT_{TRI}) are next analyzed. In the present study, the peak temperature dropped $\Delta T_{RAD} = 137$ K and $\Delta T_{TRI} = 51$ K. In similar investigations, Li and Modest [28] reported a decrease in the peak temperature of $\Delta T_{TRI} = 110$ K when comparing results without and with TRI, while Li and Modest [32] found decreases of $\Delta T_{RAD} = 145$ K and $\Delta T_{TRI} = 64$ K for a flame with an optical thickness of 0.474. The flame of the current study has an optical thickness of about 0.43, therefore with a slightly smaller influence of thermal radiation, so the differences between the studies are consistent. Coelho [51] reported that the radiative transfer led to cooler flames, especially when considering TRI, which accounted for about one-third of the total drop in the flame peak temperature of a turbulent diffusion flame of methane–air. Also, Poitou et al. [30] found drops of $\Delta T_{RAD} = 150$ K in the peak temperature for a propane–air turbulent diffusion flame.

Fig. 2(g) shows the ratio x_{H_2O}/x_{CO_2} (which is equivalent to p_{H_2O}/p_{CO_2}) inside the chamber domain, where it is noted that almost the entire chamber has a ratio close to 2.0, which is an important aspect to model the radiative properties of the medium. For a deeper understanding of this approximation, Fig. 3 shows the fraction of control volumes with different x_{H_2O}/x_{CO_2} values for two different temperature ranges: one less than 1000 K (Fig. 3(a)), and the other above 1000 K (Fig. 3(b)). Since this is an essentially emitting flame, as will be shown later in Fig. 4 and Table 6, the control volumes with temperature greater than approximately 1000 K are radiatively more important, since they are the emitting volumes, while the volumes with temperature less than 1000 K are considered as the absorbing volumes. As shown in Fig. 3(b), all control

volumes with temperatures above 1000 K have the ratio x_{H_2O}/x_{CO_2} very close to 2.0, indicating that the use of WSGG correlations obtained for a fixed $x_{H_2O}/x_{CO_2} = 2$ ratio, as seen in Table 1, is in fact a reasonable choice.

Fig. 4(a–d) shows the radiative heat source obtained for the second and third radiative scenarios, as well as the relative deviation between them, computed as (subscripts *with TRI* and *without TRI* indicate which radiative scenario was used to compute S_{rad}):

$$\% \text{Deviation} = 100 \frac{S_{rad, \text{with TRI}} - S_{rad, \text{without TRI}}}{S_{rad, \text{without TRI}}} \quad (15)$$

As with the temperature field, the radiation fields also changed significantly as a result of the different radiative scenarios (with and without TRI). TRI can contribute to increase the mean radiation intensities in turbulent non-premixed flames by 10% to more than 50% in methane or natural gas flames [51]. Fig. 4(a) and (b) shows the radiative heat source contours without and with TRI, respectively. The flame region with the highest temperatures emits more radiation than absorbs, leading to negative heat sources, while the flame region with the smallest temperatures absorbs more radiation than emits, leading to positive heat sources. To quantify the effect of including or not TRI, Fig. 4(c) shows the relative deviation of the radiative heat source obtained with the two solutions. As seen, the radiative heat source calculated with TRI was in general higher than the one without TRI. The higher differences were located at the flame core with intermediate temperature levels and negative net radiative source (emitting region). In addition, Fig. 4(d) shows S_{rad} profiles along axial direction at chamber centerline. From this figure it is observed that the inclusion of TRI increased the absolute value of the radiative heat source, as also shown in Fig. 4(a) and (b) and as corroborated by the results that will be presented later in Tables 5 and 6.

Figs. 5 and 6 show the temperature, H_2O molar fraction and CO_2 molar fraction profiles along the axial direction at the chamber centerline, and along the radial direction at an axial position of 0.912 m from the chamber entrance, considering the scenarios de-

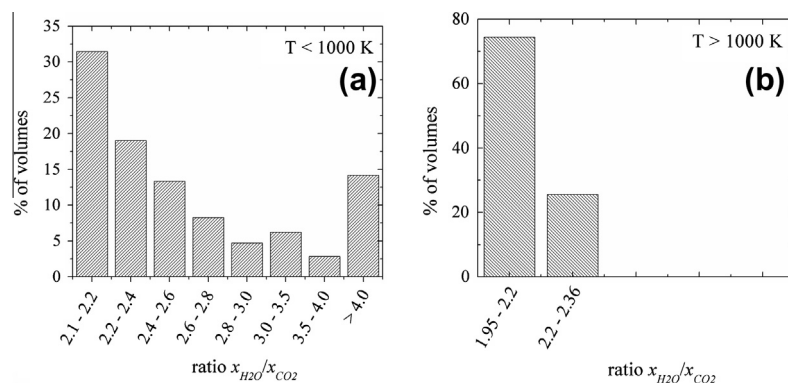


Fig. 3. Fraction of volumes in the current flame simulation within different x_{H_2O}/x_{CO_2} intervals.

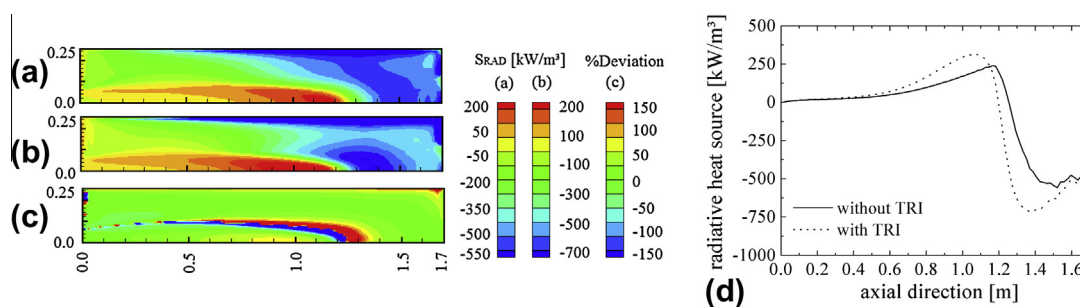


Fig. 4. Radiative heat source fields: (a) radiation computed without TRI; (b) radiation computed with TRI; (c) relative deviation between (a) and (b); and (d) axial profiles of the radiative heat source along the chamber centerline.

Table 3

Average relative deviation expressing the temperature difference between experimental data and numerical results for both radiative scenarios, in %.

	Without radiation	With radiation, without TRI	With radiation, with TRI
Axial profile (Fig. 5)	2.1	2.4	2.5
Radial profile at $z = 0.312$ m (Fig. 7)	4.6	4.4	6.2
Radial profile at $z = 0.912$ m (Fig. 6)	15.8	8.8	7.0
Radial profile at $z = 1.312$ m (Fig. 7)	12.8	4.6	1.5

Table 4

Average relative deviation expressing the CO₂ molar fraction difference between experimental data and numerical results for both radiative scenarios, in %.

	Without radiation	With radiation, without TRI	With radiation, with TRI
Axial profile (Fig. 5)	11.4	9.3	8.9
Radial profile at $z = 0.912$ m (Fig. 6)	6.4	4.8	4.4

Table 5

Heat transfer rate on the combustion chamber radial wall.

	Without radiation	Without TRI	With TRI
Convection heat transfer rate (kW)	83.0	71.1	55.7
Radiative heat transfer rate (kW)	0.00	81.6	107.7
Total rate (radiation + convection) (kW)	83.0	152.7	163.4

Table 6

Predicted net radiative heat loss and fraction of radiative heat loss.

	Net radiative heat loss (kW)	Radiant fraction (f_{rad}) (%)
Without TRI	103.3	17.1
With TRI	135.7	22.4

scribed above (neglecting radiation and considering radiation with/without TRI), together with the experimental data of Garréton and Simonin [36] (data not available for H₂O). Fig. 7 shows the temperature profiles for the same scenarios but along radial direction at axial positions of 0.312 m and of 1.312 m from the chamber entrance. One observes that the temperature values and temperature gradients decreased when radiation was considered since the heat

transfer was improved. The same behavior is observed comparing results obtained without and with TRI, that is, since computation of radiation with TRI led to higher radiative transfer in comparison to the computation without TRI, the temperature and gradients reduced when TRI was considered. The same analysis could be implied from Fig. 2. Since the reaction rate coefficients depend on the temperature, radiation should affect the formation and consumption of the species involved in the process. In spite of this, the mean variations of H₂O and CO₂ molar fractions using the different radiative scenarios were less than 1.0%, showing that the species molar fractions were considerably less affected by the radiative modeling than the temperature. This could be caused by the use of a reduced-chemistry assumption used in the present study,

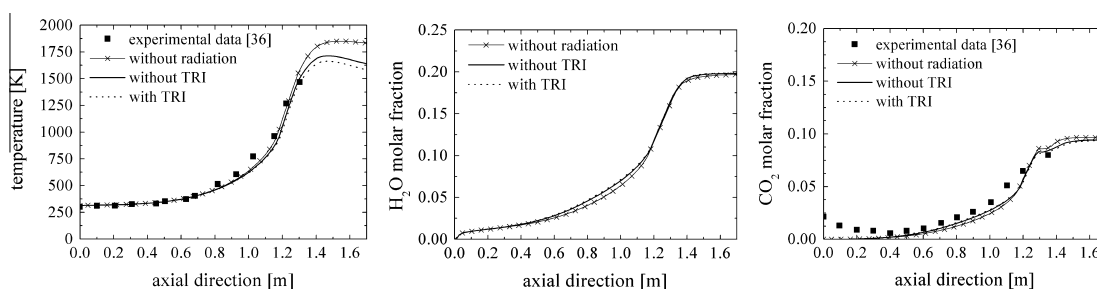


Fig. 5. Axial profiles of temperature, CO₂ and H₂O along the chamber centerline.

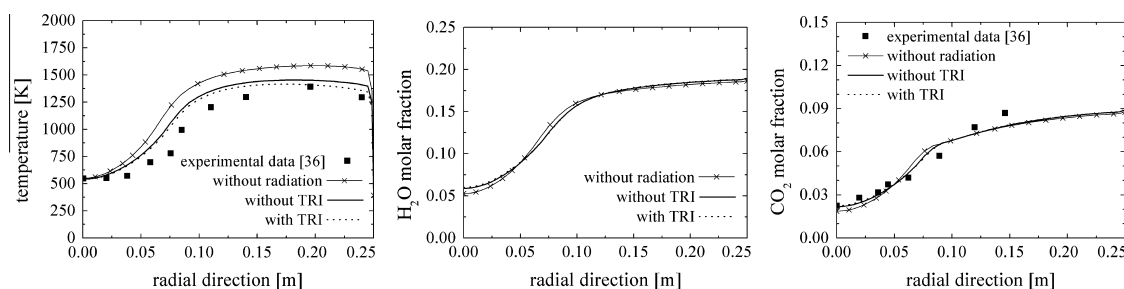


Fig. 6. Temperature, CO₂ and H₂O radial profiles at z = 0.912 m.

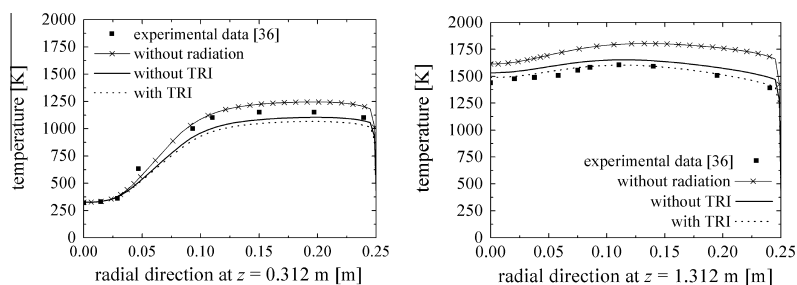


Fig. 7. Temperature radial profiles for z = 0.312 m and for z = 1.312 m.

in which chemical reaction rate is primarily controlled by turbulent mixing and, therefore, is less sensitive to temperature. On the other hand, the heat transfer rate through the chamber radial wall, the net radiative heat loss and the radiant fraction strongly depended on the radiation modeling, as revealed in Fig. 4, and Tables 5 and 6. Figs. 5–7 also show that for all the radiation scenarios, the mean temperature and mean molar fraction of CO₂ followed the experimental data trend despite some minor deviations. Those differences had probably minor relation to the choice of the radiation modeling, arising from limitations of the other models (turbulence and combustion models).

Tables 3 and 4 presents the average relative deviation, $\%Dev = \sum_{i=1}^n \frac{1}{n} |100(V_{exp,i} - V_{rad,i})/V_{exp,max}|$, which expresses the difference between the experimental data, V_{exp} , and the numerical results, V_{rad} , for all the results of Figs. 5–7. In the above relation, V can assume values of temperature or CO₂ molar fraction, and n is the total number of experimental data in each case. The deviations shown in Tables 3 and 4 indicate that the major effect of radiation is on the temperature field, especially in the radial direction profiles, with minor effect on CO₂ molar fractions, which corroborates the results shown in Figs. 5 and 6.

An additional view of the effect of thermal radiation is presented in Table 5, which shows the heat transfer rates through the chamber radial wall. The inclusion of thermal radiation has a major effect in the radiation-convection combined heat transfer mode, leading to an increase in the total heat transfer from 83.0 kW (only convection, without radiation heat transfer) to a maximum of 163.4 kW (sum of convection and radiation heat transfer for the scenario with TRI). The pattern of these results is in agreement with [37], where it was shown that the predicted heat transfer through the chamber wall was approximately doubled when radiation was taken into account (this work, however, did not consider TRI for the radiation calculations). It is interesting to note that when thermal radiation was included, as well as TRI, the convective heat transfer decreased in comparison to the scenario in which thermal radiation was neglected, since the temperature gradients in the chamber were reduced due to the increased heat transfer. The results also show that the radiation heat transfer was increased when TRI was considered, as expected since the

radiative heat source (Fig. 4) was higher in this case. The net effect of TRI was an increase in the flame radiative emission, as seen in Fig. 4(b), and since the participant gaseous medium has an optical thickness relatively thin, higher flame radiative emission led in turn to higher radiative heat fluxes through the chamber walls.

The net radiative heat loss and its normalized variable, the radiant fraction (f_{rad}), are important quantities to describe the overall radiation field of the flame. The net radiative heat loss corresponds to the integral of S_{rad} over the computational domain, while the radiant fraction is the ratio of this value to the heat released in the combustion. In all simulation scenarios, these quantities were calculated; the results are shown in Table 6. As seen, the radiation loss and the corresponding radiant fraction from the present flame achieved significant values. It is observed on Table 6 that radiant fraction increased about 31% when TRI was considered on the calculations. Such an increase is in agreement with data from literature for methane–air flames [28,32,35]. As a final comment, the overall energy balance on the combustion chamber, as well as the radiative energy balance, was strictly verified in all simulations. The differences between the radiative heat transfer rates reported in Table 5 and the net radiative heat losses reported in Table 6 were because the results in Table 5 are related only to radiative heat transfer on the radial wall of the chamber, not taking into account the annular walls located at the entrance and exit of the chamber, as well as the inlet and outlet boundaries of the chamber.

5. Conclusions

This study presented an analysis of the thermal radiation in a turbulent non-premixed methane–air flame in a cylindrical combustion chamber. The radiation field was computed with the WSGG model using recently obtained correlations [16] based on the up-to-date HITEMP2010 and considering TRI effects [35]. A two-step global reaction mechanism was used and turbulence modeling was considered via standard $k-\epsilon$ model. The RTE was solved employing the discrete ordinates method. This work showed the importance of accurate predictions of the radiative heat transfer for combustion problems by means of three scenar-

ios: radiation neglected from calculations, and radiation computed without TRI and with TRI. The comparison of the results obtained from the different scenarios showed that the temperature (especially at high temperature regions), the radiative heat source, the heat transfer through chamber wall and the radiant fraction were importantly affected by the different scenarios, while radiation had minor importance in the prediction of the chemical species concentrations for the adopted chemical reaction model. The numerical results considering radiation in the analysis were closer to the experimental data [36] when compared to the case neglecting it; the inclusion of TRI made the results even closer to the data, although the influence of including radiation (even without TRI) was more important. Also, inclusion of TRI had important influence on global results, such as the flame peak temperature and radiant fraction, in agreement with results reported in the literature for radiation-TRI simulations on methane–air flames. Some possible future advances in the radiation analysis are including kinetics for soot formation, a needed step prior to modeling combined soot and gas radiation.

Acknowledgement

The last author thanks CNPq (Brazil) for research Grants 304728/2010–1 and 473899/2011–6.

References

- [1] Hottel HC, Sarofim AF. Radiative transfer. McGraw-Hill Book Company; 1967.
- [2] Smith TF, Shen ZF, Friedman JN. Evaluation of coefficients for the weighted sum of gray gases model. *J Heat Transfer* 1982;104:602–8.
- [3] Smith TF, Al-Turki AM, Byun KH, Kim TK. Radiative and conductive transfer for a gas/soot mixture between diffuse parallel plates. *J Thermophys Heat Transfer* 1987;1:50–5.
- [4] Demarco R, Consalvi JL, Fuentes A, Melis S. Assessment of radiative property models in non-gray sooting media. *Int J Therm Sci* 2011;50:1672–84.
- [5] Watanabe H, Suwa Y, Matsushita Y, Morozumi Y, Aoki H, Tanno S, et al. Spray combustion simulation including soot and NO formation. *Energy Convers Manage* 2007;48:2077–89.
- [6] Bidi M, Hosseini R, Nobari MRH. Numerical analysis of methane–air combustion considering radiation effect. *Energy Convers Manage* 2008;49:3634–47.
- [7] Bazdidi-Tehrani F, Zeinivand H. Presumed PDF modeling of reactive two-phase flow in a three dimensional jet-stabilized model combustor. *Energy Convers Manage* 2010;51:225–34.
- [8] Yilmaz I, Taştan M, İlbaş M, Tarhan C. Effect of turbulence and radiation models on combustion characteristics in propane–hydrogen diffusion flames. *Energy Convers Manage* 2013;72:179–86.
- [9] Crnomarkovic N, Sijercic M, Belosevic S, Tucakovic D, Zivanovic T. Numerical investigation of processes in the lignite-fired furnace when simple gray gas and weighted sum of gray gases models are used. *IJHMT* 2013;56:197–205.
- [10] Yadav R, Kushari A, Eswaran V, Verma AK. A numerical investigation of the Eulerian PDF transport approach for modeling of turbulent non-premixed pilot stabilized flames. *Combust Flame* 2013;160:618–34.
- [11] Silva CV, Indrusiak MLS, Beskow AB. CFD analysis of the pulverized coal combustion processes in a 160 MWe tangentially-fired-boiler of a thermal power plant. *JBSMSE* 2010;32:427–36.
- [12] Krishnamoorthy G. A new weighted-sum-of-gray-gases model for CO₂–H₂O gas mixtures. *Int Commun Heat Mass Trans* 2010;37:1182–6.
- [13] Johansson R, Leckner B, Andersson K, Johnsson F. Account for variations in the H₂O to CO₂ molar ratio when modeling gaseous radiative heat transfer with the weighted-sum-of-gray-gases model. *Combust Flame* 2011;158:893–901.
- [14] Rothman LS, Gordon IE, Barber RJ, Dothe H, Gamache RR, Goldman A, et al. HITEMP, the high-temperature molecular spectroscopic database. *JQSRT* 2010;111:2130–50.
- [15] Kangwanpongpan T, França FHR, Silva RC, Schneider PS, Krautz HJ. New correlations for the weighted-sum-of-gray-gases model in oxy-fuel conditions based on HITEMP 2010 database. *IJHMT* 2012;55:7419–33.
- [16] Dorigon LJ, Duciak G, Brittes R, Cassol F, Galarça M, França FHR. WSGG correlations based on HITEMP 2010 for computation of thermal radiation in non-isothermal, non-homogeneous H₂O/CO₂ mixtures. *IJHMT* 2013;64:863–73.
- [17] Soufiani A. Temperature turbulence spectrum for high-temperature radiating gases. *J Thermophys* 1991;5:489–94.
- [18] Foster PJ. The relation of time–mean transmission of turbulent flames to optical depth. *J Inst Fuel* 1969;42:179–82.
- [19] Amin M, Foster PJ. Fluctuations in the transmittance of a turbulent propane jet flame. In: European symposium on combustion; 1973. p. 530–5.
- [20] Tan E, Foster PJ. Radiation through a turbulent medium. In: 6th International heat transfer conference; 1978. p. 403–8.
- [21] Hall RJ, Vranos A. Efficient calculations of gas radiation from turbulent flames. *IJHMT* 1994;37(17):2745–50.
- [22] Krebs W, Koch R, Bauer HJ, Kneer R, Wittig S. Effect of turbulence on radiative heat transfer inside a model combustor. In: Eurotherm seminar no. 37 – heat transfer in radiating and combusting systems 2, 1994. p. 349–62.
- [23] Krebs W, Koch R, Ganz B, Eigenmann L, Wittig S. Effect of temperature and concentration fluctuations on radiative heat transfer in turbulent flames. In: 26th Symposium (international) on combustion; 1996. p. 2763–70.
- [24] Coelho PJ. Evaluation of a model for turbulence/radiation interaction in flames using a differential solution method of the radiative transfer equation. In: 12th International heat transfer conference; 2002. p. 705–10.
- [25] Coelho PJ. Detailed numerical simulation of radiative transfer in a non-luminous turbulent jet diffusion flame. *Combust Flame* 2004;136:481–92.
- [26] Kabashnikov VP, Kmit GL. Influence of turbulent fluctuations on thermal radiation. *J App Spectrosc* 1979;31:963–7.
- [27] Song TH, Viskanta R. Interaction of radiation with turbulence: application to a combustion system. *J Thermophys* 1987;1(1):56–62.
- [28] Li G, Modest MF. Application of composition PDF methods in the investigation of turbulence–radiation interactions. *JQSRT* 2002;73:461–72.
- [29] Habibi A, Merci B, Roekaerts D. Turbulence radiation interaction in Reynolds-averaged Navier–Stokes simulations of nonpremixed piloted turbulent laboratory-scale flames. *Combust Flame* 2007;151:303–20.
- [30] Poitou D, Amaya J, El Hafi M, Cuénot B. Analysis of the interaction between turbulent combustion and thermal radiation using unsteady coupled LES/DOM simulations. *Combust Flame* 2012;159:1605–18.
- [31] Gupta A, Haworth DC, Modest MF. Turbulence–radiation interactions in large-eddy simulations of luminous and nonluminous nonpremixed flames. *Proc Combust Inst* 2013;34:1281–8.
- [32] Li G, Modest MF. Importance of turbulence–radiation Interactions in turbulent reacting flows. In: Proceedings of 2002 ASME IMECE; 2002.
- [33] Habibi A, Merci B, Roekaerts D. The importance of turbulence–radiation interaction in RANS simulations of a turbulent non-premixed laboratory-scale bluff-body flame. In: 3rd European combustion meeting; 2007.
- [34] Modest MF, Mehta RS. Modeling absorption TRI in optically thick eddies. In: Eurotherm 78 – computational thermal radiation in participating media II; 2006.
- [35] Snegirev AY. Statistical modeling of thermal radiation transfer in buoyant turbulent diffusion flames. *Combust Flame* 2004;136:51–71.
- [36] Garréton D, Simonin O. Final results. In: Proceedings of the 1th workshop of aerodynamics of steady state combustion chambers and furnaces, vol. 25, 1994. p. 29–35.
- [37] Silva CV, França FHR, Vielmo HA. Analysis of the turbulent, non-premixed combustion of natural gas in a cylindrical chamber with and without thermal radiation. *Combust Sci Technol* 2007;179:1605–30.
- [38] Magel HC, Schnell U, Hein KRG. Modeling of hydrocarbon and nitrogen chemistry in turbulent combustor flows using detailed reaction mechanisms. In: Proceedings of the 3rd workshop on modeling of chemical reaction systems; 1996.
- [39] Niecele AO, Naccache MF, Gomes MSP, Carneiro JE, Serfaty R. Models evaluations of combustion process in a cylindrical furnace. In: Proceedings of 2001 ASME IMECE; 2001.
- [40] Patankar SV. Numerical heat transfer and fluid flow. Washington, DC: Hemisphere; 1980.
- [41] Spalding DB. Combustion and mass transfer. New York: Pergamon Press; 1979.
- [42] Eaton AM, Smoot LD, Hill SC, Eatough CN. Components, formulations, solutions, evaluations and applications of comprehensive combustion models. *Prog Energy Combust Sci* 1999;25:387–436.
- [43] Turns SR. An introduction to combustion: concepts and applications. McGraw-Hill; 2000.
- [44] Fluent Incorporated. FLUENT theory guide; 2009.
- [45] Magnussen BF, Hjertager BH. On mathematical models of turbulent combustion with special emphasis on soot formation and combustion. In: Proceedings of the 16th symposium (international) on combustion – The Combustion Institute; 1977. p. 719–29.
- [46] Woolley RM, Yunardi MF. Conditional moment closure modelling of soot formation in turbulent, non-premixed methane and propane flames. *Fuel* 2009;88:393–407.
- [47] Mehta RS. Detailed modeling of soot formation and turbulence–radiation interactions in turbulent jet flames. The Pennsylvania State University, PhD Thesis; December 2008.
- [48] Modest MF. The weighted-sum-of-gray-gases model for arbitrary solution methods in radiative transfer. *ASME J Heat Transfer* 1991;113:650–6.
- [49] Centeno FR, Cassol F, Vielmo HA, França FHR, Silva CV. Comparison of different WSGG correlations in the computation of thermal radiation in a 2D axisymmetric turbulent non-premixed methane–air flame. *JBSMSE* 2013;35:419–30.
- [50] Coelho PJ, Teerling OJ, Roekaerts D. Spectral radiative effects and turbulence/radiation interaction in a non-luminous turbulent jet diffusion flame. *Combust Flame* 2003;133:75–91.
- [51] Coelho PJ. Numerical simulation of the interaction between turbulence and radiation in reactive flows. *Prog Energy Combust Sci* 2007;33:311–83.
- [52] Burns SP. Turbulence radiation interaction modeling in hydrocarbon pool fire simulations. Sandia Report SAND 99–3190; 1999.